The Spatiotemporal Structure of 20th Century Climate Variations in Observations and Reanalyses. Part II: Pacific Pan-Decadal Variability

Junye Chen[1,2], Anthony D. Del Genio[3], Barbara E. Carlson[3], Michael G. Bosilovich[2]

[1]Earth System Science Interdisciplinary Center
University of Maryland, College Park
College Park, Maryland

[2]Global Modeling and Assimilation Office
NASA Goddard Space Flight Center
Greenbelt, Maryland

[3]NASA Goddard Institute for Space Studies
New York, New York

Submitted to Journal of Climate
April 19, 2007

Revised October 10, 2007

Corresponding author:
Junye Chen
NASA/GSFC Code 610.1
Greenbelt, MD 20771-0001
Phone: 301-614-6173
Email: jchen@gmao.gsfc.nasa.gov

ABSTRACT

The spatiotemporal structure of Pacific pan-decadal variability (PDV) is isolated in global long-term surface temperature (ST) datasets and reanalysis atmospheric parameter fields from which El Niño-Southern Oscillation (ENSO) effects have been removed. Empirical orthogonal function (EOF) and combined EOF analysis of the resulting time series identify PDV as one of two primary modes of long-term variability, the other being a global warming (GW) trend which is addressed in a companion paper (Part I).

In this study, we show that one of several PDV interdecadal regime shifts occurred during the 1990s. This significant change in the Pacific basin is comparable but anti-phase to the well-known 1976 climate regime shift, and is consistent with the observed changes in bio-systems and ocean circulation. A comprehensive picture of PDV as manifested in the troposphere and at the surface is described. In general, the PDV spatial patterns in different parameter fields share some similarities with the patterns associated with ENSO, but important differences exist. First, the PDV circulation pattern is shifted westward by about 20° and is less zonally extended than that for ENSO. The westward shift of the PDV wave train produces a different North American teleconnection pattern that is more west-east oriented. The lack of a strong PDV ST signal in the west equatorial Pacific and the relatively strong ST signal in the subtropical regions are consistent with an atmospheric overturning circulation response that differs from the one associated with ENSO. Our analysis also suggests that PDV is a combination of decadal and/or interdecadal oscillations interacting through teleconnections.

1. Introduction

In addition to the interannual El Niño-Southern Oscillation (ENSO) phenomenon, strong climate variability on decadal and interdecadal time scales also exists in the Pacific basin. In this study, we refer to this longer-term climate variability as the Pacific pan-decadal variability (PDV); it has also been referred to as the Pacific decadal oscillation (PDO), interdecadal Pacific oscillation (IPO), ENSO-like interdecadal variability, or Pacific interdecadal variability. PDV is characterized by an ENSO-like spatial pattern (Zhang et al. 1997), multiple oscillation periods (Minobe 2000; Tourre et al. 2001; Mantua and Hare 2002), and abrupt phase changes marked as climate regime shifts (Nitta and Yamada 1989; Trenberth 1990).

Recognition of the existence of PDV has been a gradual process. In the late 1980s, the climate research community began to realize that a climate regime shift had occurred in the North Pacific in 1976-77, characterized by a strengthened and eastward-shifted Aleutian low-pressure system, anomalous cooling in the Central North Pacific, and warming along the west coast of North America (Nitta and Yamada 1989; Trenberth 1990). In the mid-1990s, it was found that the 1976–77 North Pacific regime shift was coincident with an El Niño-like shift in the background state in the tropical Pacific region (Graham 1994; Trenberth and Hurrell 1994). Through analysis of tropical and Northern Hemisphere data of longer duration, it was realized that the 1976-77 regime shift was not unique in the last century. In fact, similar shifts occurred around 1925 and 1943. Such shifts are the manifestations of the abrupt phase changes of the interdecadal ENSO-like ocean-atmosphere variability in the Pacific Ocean (Zhang et al. 1997; Mantua et al. 1997). Later, Garreaud and Battisti (1999) expanded the study of Zhang et al. (1997) to

the Southern Hemisphere based on NCEP/NCAR reanalysis products.

A variety of possible mechanisms have been proposed to explain the pan-decadal climate variations in the Pacific Ocean; Latif (1998) and Miller and Schneider (2000) review the proposed mechanisms. In these reviews, the North Pacific region is emphasized over other regions. Four possible PDV mechanisms are broadly considered as follows. First, stochastic atmospheric forcing can redden the sea surface temperature (SST) spectrum, thus stimulating long-term climate variability (Frankignoul and Hasselmann 1977).

The second mechanism is the tropical delayed oscillator mechanism (Knutson and Manabe 1998; White et al. 2003), which is similar to the dynamics of ENSO but with an expanded latitude range. The expanded latitude range seems consistent with a longer time scale as the propagation speed decreases quickly with the increase of latitude (Fyfe and Saenko 2007). At the same time, the equatorial coupled wave speed associated with decadal oscillation also appears slow in model simulations (White et al. 2003). The tropical anomaly can be transported to higher latitudes through atmospheric teleconnections, which manifest as the Pacific-North American (PNA) and Pacific-South American (PSA) patterns, similar to the way in which the ENSO signal spreads.

Tropical-midlatitude decadal interaction is the third proposed mechanism. Anomalous SST in the equatorial East Pacific produces an anti-phase anomaly of SST in the Central Pacific at high latitudes through atmospheric teleconnections. Instead of being a passive actor, the SST anomaly at high latitudes subducts to low latitudes along the mean thermocline circulation on the decadal time scale, emerges to the surface, and changes the phase of the SST anomaly in the east equatorial region to complete the circle of decadal

oscillation (Gu and Philander 1997).

The fourth mechanism is localized in the North Pacific. In the central North Pacific, anomalous SST will cause the atmosphere to react in a PNA (PSA in the Southern Hemisphere) pattern. This is related to the anomalous heat flux exchange at the sea surface, which enforces the original SST anomaly (a positive feedback). The wind stress curl anomaly associated with the PNA pattern causes a delayed change of the speed of the subtropical gyre circulation many years later, consequently changing the poleward ocean heat flux along the western boundary current and reducing the original Central North Pacific SST anomaly (a delayed negative feedback), thus causing the decadal oscillation (Latif and Barnett 1996). In model simulations, the signal of the decadal variability at high latitudes is also apparently transported to the tropics through atmospheric teleconnections (Barnett et al. 1999; Liu and Yang 2003).

It is still unclear which mechanism is the dominant cause of PDV. Recent studies suggest inter-basin interaction on decadal and longer time scales, emphasizing the relationship between the North Atlantic and Pacific through air-sea coupling and atmospheric teleconnection (Wu et al. 2005), and the global oceanic teleconnection initiated by the variation of the North Atlantic thermohaline circulation (Timmermann et al. 2005). Other studies argue that PDV is a combination of several decadal and interdecadal oscillations that originate from these mechanisms (Enfield and Mestas-Nunez 1999; Liu et al. 2002; Wu et al. 2003). The inconclusive situation is due to both the complexity of PDV itself and the lack of a comprehensive, precise observational depiction of PDV (Latif 1998; Miller and Schneider 2000).

The gradual recognition of PDV and the difficulty understanding it stem from the

short record of climate data, the absence of a definitive model, and the fact that the PDV signal is blurred by signals produced by other climate phenomena, especially the dominant interannual ENSO phenomenon and the long-term global warming (GW) trend in the 20th century. Smoothing data with a window of around six to eight years can minimize the effects of ENSO. But this pretreatment forfeits the chance to detect a possible regime shift earlier than six years after it occurs; it also excludes observational datasets of relatively short duration from being used to investigate PDV. Linear detrending at each grid or removing the global mean trend at each grid are common methods of diminishing the effect of the GW trend. However, as shown in Chen et al. (2007, which is a companion to this paper, and referred to as Part I hereafter), the global mean trend is not linear, and the warming is unevenly spatially distributed.

The ENSO-removal method developed in Chen (2005, also described in Appendix A of Part I) provides a new means to investigate long-term climate variations. It is based on the fact that the ENSO signal spreads from the tropical Pacific to remote regions with different time delays. In this research, the PDV phenomenon is isolated in EOF analyses based on surface temperature (ST) and reanalysis tropospheric parameter fields from which ENSO effects have been subtracted. Two long-term global ST datasets are used. One is the extended reconstruction of global SST version 2 (ERSST.V2) (Smith and Reynolds 2003; Smith and Reynolds 2004), the other is the NASA GISS surface temperature (GISTEMP) analysis (Hansen et al. 1999). In addition to the two ST datasets, 5 atmospheric parameters (air temperature (T_{air}), zonal wind speed (U), meridional wind speed (V), vertical velocity (ω), specific humidity (q)) at 8 pressure levels (1000hPa, 925hPa, 850hPa, 700hPa, 600hPa, 500hPa, 400hPa, 300hPa) from the NCEP/NCAR

(Kalnay et al. 1996, Kistler et al. 2001) and ERA-40 (Uppala et al. 2005) reanalyses are analyzed. Detailed descriptions of the datasets and analysis procedures we use are given in Section 2 of Part I. The principal components (PC) representing the time evolution of PDV suggest that a new phase shift occurred in the 1990s that is comparable to but anti-phase from the 1976 phase shift. The derived spatial patterns of the ST fields reveal new characteristics of PDV. The comprehensive structure of PDV in different parameter fields at different levels of the atmosphere helps us to understand the atmospheric processes associated with the PDV phenomenon.

In the next section, the spatiotemporal structure of PDV manifested in the ST field is discussed. In Section 3, we investigate PDV characteristics in atmospheric parameter fields. ENSO is used as a reference for comparison to investigate the unique characteristics of PDV in both sections. Section 4 provides clues to the dynamics of PDV through comparison among regional analyses of SST in the North Pacific, tropical Pacific, and South Pacific. Conclusions and implications for the interpretation of recently observed climate variations are discussed in Section 5.

2. The Pacific pan-decadal variability manifested in the ST field

After the GW trend mode, PDV appears as the second mode in the ERSST.V2 (ocean-only) ENSO-removed EOF analysis and the third mode[*] in the GISTEMP (ocean + land) ENSO-removed EOF analysis. The PDV mode for both analyses is shown in Figure 1. The PC time series capture three known significant regime shifts in 1925, 1943,

[*] The second mode in the GISTEMP ENSO-removed EOF analysis is a long-term variation that occurred in the high latitude Eurasia region. It does not appear in the analysis based on the 45°S-45°N spatial range. We will not address this high latitude variation in detail, because this study is only concerned with middle and low latitudes. Our analysis is not ideally suited to studying other known modes of natural variability such as the Arctic, North Atlantic, and Antarctic Oscillations because we exclude latitudes poleward of 60°, although we cannot rule out the possibility that these contribute to some of the higher order modes we find.

and 1976. The EOF spatial patterns address the ENSO-like nature of PDV: the SST anomaly over the tropical Pacific and off the west coast of both North and South America is out of phase with the SST anomaly over the middle latitudes of the Pacific in both hemispheres.

As shown in Figure 1, because the PDV signals in high and low latitudes are out of phase and thus offset each other, the global mean temperature change (Figure 1, top) associated with the PDV phenomenon is in the range of ±0.02K, which is negligible compared with the approximately 0.8K value of the GW trend mode and the approximately ±0.2K value of the ENSO phenomenon (Figure 1 in Part I). Though the absolute value is small, the PDV effect on the global mean temperature in the ERSST.V2 analysis is about –1.5 times that of the GISTEMP analysis. In the ERSST.V2 analysis, the global mean temperature change associated with PDV is negative after 1977; however, in the GISTEMP analysis, the global mean ST change associated with PDV is positive after 1977. The reason for this difference is the disagreement between the two datasets, not the inclusion of land regions in the GISTEMP analysis, i.e., warm regional anomalies slightly outweigh cool anomalies in GISTEMP but vice-versa for ERSST.V2. The sign obtained from an ocean-only analysis based on GISTEMP is the same as from the original GISTEMP analysis.

From the PC time series in Figure 1, we can see abrupt changes over the course of the 20th century. The time interval for these changes usually is around or less than 10 years. Bidecadal to multidecadal variability is superimposed on this decadal time scale variability (Minobe, 1999). The three events occurring in 1925, 1943, and 1976 are broadly thought of as climate regime shifts (Zhang et al. 1997; Mantua et al. 1997),

because the PDV is inclined to persist in one state for several decades after these three events.

Another dramatic phase change occurred from the mid- to late 1990s. Though the PC time series begins to decline after 2000 and the GISTEMP time series (Figure 1, top, black) even drops below zero in 2003, the 1990s event may turn out to have been a regime shift because, unlike the change that occurred in 1989, the peak in late 1999 reaches an amplitude comparable to those peaks between 1945 and 1975, suggesting a possible phase change on the interdecadal time scale. At the same time, the 1990s event coincides with dramatic interdecadal changes in the Pacific biosystem (Chavez et al. 2003) and ocean circulation (McPhaden and Zhang 2004). According to an analysis based on the Zebiak-Cane model, the interdecadal warm phase of the tropical Pacific since 1976 ends after the 1998 El Niño (Seager et al. 2004).

Compared with the global mean, the regional ST change associated with PDV is much larger (of order 1.5K) in several regions of the Pacific basin. In the middle and bottom panels of Figure 1, a strong positive signal appears in the North Pacific and in a long zonal band from New Zealand to the Southeast Pacific; a strong negative signal appears in a broad area from the equatorial Central Pacific to the Eastern Pacific. The negative feature gradually expands its latitude range in both hemispheres from the Central Pacific to the Eastern Pacific, reaching high latitudes along the west coast of North and South America.

The spatial character of PDV is roughly like that of ENSO (Figure 2), but there are significant differences. First, the regional signal of ENSO is generally stronger than that of PDV, even in the Indian Ocean and Atlantic Ocean. In the study of Garreaud and

Battisti (1999), the ENSO signal is weaker than the PDV signal in the Indian Ocean and the Atlantic Ocean. The reason for this difference is unclear. One possibility is that our study includes the effect of the time lag of the ENSO signal spreading outside of the Pacific, while Garreaud and Battisti's study obtains the ENSO signal from a simultaneous regression.

To show the regional relative strength of the ENSO and PDV signals, we map the difference between the absolute values of the standardized ENSO and PDV signals from GISTEMP (|ENSOsG|-|PDVsG|) in the bottom left panel of Figure 2. The ratio of |ENSOsG|-|PDVsG| to |PDVsG-PDVsE| (absolute value of the difference between the standardized PDV signal from GISTEMP and ERSST.V2) (Figure 2, bottom right) shows the significant differences between the ENSO and PDV spatial patterns relative to the uncertainty in the PDV signal from different datasets. In both bottom panels of Figure 2, a positive (negative) value means that the regional ENSO signal is relatively strong (weak), and the regional PDV signal is relatively weak (strong).

There are several important regional differences between the ENSO and PDV spatial patterns as shown in Figure 2. First, the PDV signal in the equatorial West Pacific region is very weak, but the ENSO signal in the same area is strong and has an opposite sign from that of the Eastern Pacific, thus constructing an east-west dipole in the tropical Pacific region. Second, the maximum of the East Pacific cold tongue feature associated with ENSO is more confined near the equator while the PDV extends more to the subtropics (Zhang et al. 1997), tilting slightly in the direction of northwest-southeast between the equator and 10°S (Figure 1). Third, the PDV signal over the Southeast Aleutian Islands is stronger and extends westward to Japan, but the ENSO signal in the

same region is relatively weaker and has no significant westward extent. Fourth, in the south subtropical region, the maximum PDV signal is over New Zealand, but the maximum ENSO signal is in the band from 160°W to 120°W.

Outside of the Pacific basin, the PDV signal is significant in North America and Northern Europe (Figure 2). These PDV signals differ from the ENSO signal. If the 1990s PDV phase change is a regime shift lasting for several decades as was the 1976 event, then the spatial pattern shown in the upper panel of Figure 2 suggests that Eastern North America and Northern Europe will have a tendency to be relatively warm, and Western North America will be relatively cool in the coming decades, by about 1.0°C, in the absence of other persistent changes in climate. These PDV signals over the northern continents are consistent with the PDV (ENSO-like Interdecadal Variability) cold season surface air temperature continental features shown in Fig. 14 of Zhang et al. (1997). Mantua et al. (1997) note the PDV signal in North America but not in Northern Europe; the reason for the difference is unknown. One possibility is that the PDV (PDO) index used in Mantua et al. (1997) is the leading mode PC of the EOF based on the North Pacific SST anomaly without removal of the ENSO signal. The specific features of PDV in the ST field are consistent with the atmospheric variations shown in the next section.

3. Atmospheric variations associated with PDV

Most previous research associated with PDV is based on the ST record, which spans a relatively long time period (more than 100 years) and is of sufficiently high quality for climate analysis. In a few studies, the atmospheric changes related to PDV are obtained with a regression or correlation method, based on a PDV index derived from the ST field

(Zhang et al. 1997; Garreaud and Battisti 1999) or sea level pressure (Trenberth and Hurrell 1994). In our study, the PDV phenomenon emerges independently as the second modes in two ENSO-removed combined EOF analyses based on the NCEP/NCAR reanalysis and ERA-40 reanalysis. As addressed in Part I, these combined EOF analyses (NCEP1-40p and ERA40-40p) are based on five atmospheric parameters at eight pressure levels over the periods of 1970–2003 and 1970–2002. The second mode PCs are shown in Figure 3 along with the 1970–2003 segments of the PDV mode PCs based on the ERSST.V2 and GISTEMP ST analyses. Although based on different datasets, the four PDV mode PCs share the most significant features: dramatic changes around the mid-1970s and mid- to late 1990s.

The PDV phase change during the 1990s appears to occur in two steps: 1994 to 1996 and 1997 to 1998; the latter appears to be more dramatic. The time of the first step (1994) is coincident with the rebound of the wind-driven ocean meridional overturning circulation between the tropics and subtropics in the Pacific Ocean from a slowing trend that existed from the 1970s (McPhaden and Zhang 2002, 2004). It is also coincident with a decadal change in cloud radiative forcing in the tropics (Allan et al. 2002).

The time of the second step overlaps with the 1997–98 El Niño. Though it is possible that the 1997–98 PDV phase change and the 1997–98 El Niño are related (Seager et al. 2004), their different temporal evolutions suggest that they are not the same. The 1997-98 El Niño decays quickly in late 1998 (Figure 3 lower), while the PDV PCs (Figure 3 upper) remain in the positive regime for several years. At the same time, the PDV phase change, which moves from an El Niño-like state to a La Niña-like state, has a spatial pattern that is opposite from that of El Niño. On long time scales, the PDV PCs are not

well-correlated with the N34h index. The correlation coefficient between the N34h index and the GISTEMP (ERSST.V2) PDV PC (1900–2003) is -0.1 (-0.1), and the maximum cross-correlation is -0.2 (-0.19) at 9 (10) months lag. The maximum cross-correlation between the N34h index and the NCEP1-40p (ERA40-40p) PDV PC is only -0.1 (-0.2) at 8 (8) months lag, and does not reach the 95% confidence level. For comparison, the maximum cross-correlations between the N34h index and the first four PCs of the original time series, which are similar to the NCEP1-40p (1970-2003) analysis but without ENSO-removal, are -0.72, -0.32, 0.52, 0.41, at -1, 1, -5, 4 months lag, respectively. All are statistically confident above the 95% confidence level. This supports our conclusion that there is almost no ENSO signal included in the PDV modes of the GISTEMP, ERSST.V2, NCEP1-40p, and ERA40-40p analyses when our ENSO removal technique is applied.

The PDV PCs from the reanalyses (Figure 3 upper, black and red lines) have less intradecadal signal than the PDV PCs from the ST data (Figure 3 upper, green and blue lines). The PDV PCs from NCEP1-40p and ERA40-40p appear smoother and remain negative from the 1976 regime shift through the late 1990s, although the PDV PCs from GISTEMP and ERSST.V2 cross the zero line temporarily several times during this period. After the phase change of the 1990s, the PDV PCs from NCEP1-40p and ERA40-40p remain positive, implying that this is an interdecadal phase change similar but anti-phase to the 1976 regime shift.

The spatial pattern correlations for each atmospheric parameter between ENSO and PDV are shown in Table 1 (based on NCEP/NCAR data) and Table 2 (based on ERA-40 data). The significant but moderately low correlation values imply non-negligible

differences in the atmospheric spatial patterns between PDV and ENSO for both datasets. For comparison, the spatial pattern correlations between NCEP/NCAR and ERA-40 are shown for ENSO in Table 3 and for PDV in Table 4. The high correlation and low deviation in Table 3 demonstrate that the ENSO signal is stable and well-addressed in both datasets. Compared to the correlations in Tables 1 and 2, the correlations in Table 4 are only moderately higher, but still there are marginally more similarities between the PDV patterns based on different reanalysis datasets than between the PDV and ENSO patterns based on the same dataset. At the same time, Table 4 correlation values are low in the omega (ω) fields in the low to middle troposphere and in the specific humidity (q) fields in the upper troposphere.

A comprehensive comparison between ENSO and PDV in the atmospheric spatial patterns is shown in Figures 4, 5, and 6 for dynamics, temperature, and humidity fields, respectively. In each figure, mean ENSO patterns from both reanalyses are shown in the left column, and mean PDV patterns are shown in the right column. In the dynamics fields, both ENSO and PDV horizontal wind fields at the 300hPa level (Figure 4) show a clear wave train feature in the Pacific basin from low latitudes to high latitudes in both hemispheres. The wave train source is usually attributed to strong upper troposphere divergence (when in La Niña-like status), or convergence (when in El Niño-like status) in the subtropical regions (Trenberth et al., 1998). It is clear that neither the locations nor the shape of the wave trains of PDV and ENSO are exactly the same: the PDV wave trains are shifted about 20° westward and are less extended in the zonal direction.

In the 500hPa ω patterns (Figure 4, middle), the overturning features significantly differ between ENSO and PDV. This is also seen in the low ω correlations (typically

0.2~0.3) in Tables 1 and 2. The dominant cool phase ENSO overturning pattern (Figure 4, middle left) is a strong subsidence feature extending over the equator from west of the Central Pacific to the Eastern Pacific; strong ascending regions surround the subsidence feature to the west, northwest, and southwest. This pattern manifests the east-west shift of the convection center over the equator in different phases of ENSO. On the other hand, there is no dominant center in the PDV overturning pattern (Figure 4, middle right). The ascending feature over the Indonesian region is weak and less spatially coherent in the NCEP1-40p and ERA40-40p analyses; the subsidence feature over the equator appears to be less zonally extended and shifted west in comparison with the ENSO pattern; the ascending features in the west and descending features in the east over the subtropical regions of both hemispheres become more important.

The PDV signal in the 500hPa ω pattern (Figure 4, middle right) is strong off the coast of Chile and in eastern Brazil (positive, descending), while anomalous ascent occurs over much of the rest of South America as well as the East Pacific Intertropical Convergence Zone. These features are robust in both the NCEP1-40p and ERA40-40p analyses. However, the ST anomalies in the GISTEMP PDV pattern (Figure 2, top) disagree with the reanalyses-mean low-level temperature signal over both eastern South America and western North America (Figure 5, lower right). The South American PDV dynamical feature (Figure 4, right) also significantly differs from the corresponding feature associated with ENSO (Figure 4, left). The ENSO pattern is consistent with the PSA teleconnection pattern, the main mechanism causing ENSO climate variations in South America (Mo and Paegle, 2001). Previous studies (Garreaud and Battisti, 1999; Mo, 2000) suggest that the decadal variation in the South Pacific and South America

shares a similar PSA pattern with ENSO, but this is not the case in our analysis for reasons that are unclear.

The T_{air} patterns from PDV (Figure 5, right) and ENSO (Figure 5, left) all change from a ST like pattern to a wave train like pattern with increasing altitude. This change with altitude is natural: at the lower levels, the T_{air} is well-coupled with the surface; at the higher levels, the T_{air} is controlled by the adiabatic heating (cooling) from descending (ascending) motion corresponding to upper level convergence (divergence) that appears alternately in the wave train. However, the ENSO patterns are relatively symmetric about the equator, probably because ENSO is rooted in the equatorial Pacific, while the PDV patterns are generally stronger in the Northern Hemisphere than in the Southern Hemisphere. Near the surface, the PDV cooling maximum in the East Pacific is not over the equator (as in the ENSO pattern) but rather over the north subtropical region.

This cooling maximum and the warming maximum south of the Aleutian Islands form a dipole corresponding to the North Pacific subtropical gyre circulation. In the Southern Hemisphere, the warming over New Zealand seems to be the major feature at all levels. This is consistent with the ST patterns (Figure 1, middle and bottom). In the East Pacific from the equator to the southern subtropics, the near surface T_{air} signal is relatively weak, compared with the North Pacific subtropical signal. This is unlike the 1900–2003 GISTEMP and ERSST.V2 ST patterns (Figure 1, middle and bottom), which have strong cooling along and south of the equator. In the PDV ST pattern obtained from the ENSO-removed 1970–2003 GISTEMP EOF analysis, however, this cooling is much weaker than in the 1900–2003 analysis.

As already shown in the dynamical fields (Figure 4, top), the PDV patterns are less

zonally extended and shifted approximately 20° westward in the tropics and subtropics, in comparison with the ENSO patterns. This is also shown in the middle and upper level T_{air} fields (Figure 5). The difference in the shape and location of the wave trains affects the ST fields over midlatitude continents in the Northern Hemisphere, especially North America (Figure 2). In the PDV pattern, the less zonally extended wave train propagates more eastward than northward in midlatitudes (Figure 5), thus producing an east-west ST dipole over North America (Figure 2, top), compared to the north-south ST gradient anomaly corresponding to ENSO (Figure 2, middle).

At near surface levels, the *q* patterns for both PDV (Figure 6, right) and ENSO (Figure 6, left) resemble the associated T_{air} change, implying little effect on relative humidity. In the middle to upper troposphere, the *q* change depends more on the ω field in both patterns. For ENSO, the dominant feature in the middle to upper troposphere is the west-east dipole, one part in the Indonesian region and the other in the central to east equatorial Pacific. They represent the anomalous convection center shifting back and forth between these two regions when ENSO shifts between El Niño and La Niña, thus moistening the troposphere over one region but drying the troposphere over the other region. The PDV *q* patterns (Figure 6, right) in the middle to upper troposphere are also directly related to anomalous ascending and descending motions. The areas of strong ascent, including the area from East Asia to north of Hawaii and the area from South Indonesia to New Zealand, are moistened at all levels. The areas of strong descent, including the East Pacific subtropics and East Brazil, are dried in the middle to upper troposphere. However the upper troposphere *q* anomaly is inconsistent between NCEP1-40p and ERA40-40p (not shown). There is a drying tendency in NCEP1-40p but a

moistening tendency in ERA40-40p in the upper troposphere. This may be important for anomalies in the earth's radiation energy budget, due to the high sensitivity of the radiation flux to upper troposphere water vapor variations and related high cloud changes (Chen et al. 2002).

4. Regional analyses based on ERSST.V2

In previous sections, the PDV phenomenon was investigated near-globally based on analyses over 60°S-60°N latitude range. Because there are multiple hypotheses for the dynamical source of PDV, we now conduct an analysis based on SST in regional domains. In proposed theories, the PDV dynamical source is in the North Pacific (Latif and Barnett, 1996), tropical Pacific (Knutson and Manabe, 1998; White et al. 2003), or results from an interaction between tropical and middle latitudes (Gu and Philander, 1997). Giese et al. (2002) emphasize the possible key role of the South Pacific in the PDV.

We perform the regional analyses using the 1900–2003 ENSO-removed ERSST.V2 SST data. We pretreat the data by removing the GW trend signal, represented by the first mode of the EOF analysis based on ENSO-removed ERSST.V2 for the 60°S-60°N latitude band (see Part I). Next, we apply EOF analysis to the pretreated ERSST.V2 data in the South Pacific (60°S-20°S, S62), tropical Pacific (20°S-20°N, M22), and North Pacific (20°N-60°N, N26). The resulting EOF spatial patterns of the first modes are shown in Figure 7 along with the original PDV spatial pattern based on the ENSO-removed 60°S-60°N (M60) EOF analysis. The regional EOF spatial patterns (Figure 7, lower panels) are nearly identical to the corresponding regional features in the original

M60 spatial pattern (Figure 7, upper panel). The regional PC time series are also similar to the PC time series of the original M60 PDV mode (Figure 8, top).

However, each region has its own temporal character. The tropical Pacific (M22) and South Pacific (S62) PCs have maximum power at about 13 years (Figure 8, middle), similar to that for M60. The North Pacific (N26) PC has maximum power at about 25 years. Due to the limited time length of the data, our analysis does not exclude the possibility that PDV has significant power at periods longer than 25 years. Thus, the PDV time scale is more decadal in the tropics and South Pacific and more multi-decadal in the North Pacific. For the original M60 PDV PC time series, the maximum power is at 13 years, but there is also significant power at 25 years. In the lead-lag relationships among the PCs (Figure 8, lower panels), M22 and S62 are almost simultaneous, and they both lead N26 by several months. So, the tropical and South Pacific appear to be more tightly coupled to each other and both oscillate on the decadal time scale. The North Pacific is less coupled to the other regions; it lags the tropical and South Pacific by several months and oscillates more on a bidecadal time scale. This suggests that the PDV may consist of at least two variation components: one in the North Pacific and the other in the tropical South Pacific.

5. Discussion and concluding remarks

In this study, we isolate the PDV phenomenon in global long-term ST datasets and reanalysis fields through EOF and combined-EOF analyses after the removal of ENSO anomalies. It is suggested that a PDV interdecadal regime shift occurred during the 1990s; this shift is clearly shown in the EOF PC time series, especially in the NCEP1-40p

and ERA40-40p PCs, which are affected less by the intradecadal signal of PDV. This significant change in the Pacific basin is comparable (but anti-phase) to the well known 1976 regime shift and is consistent with the observed change in the Pacific bio-system (Chavez et al. 2003) and in the ocean circulation (McPhaden and Zhang 2004).

Our analyses of the ST and the atmospheric parameter fields provide a comprehensive picture of the PDV phenomenon as manifested in the atmosphere and at the surface. The changes associated with PDV are consistent in the T_{air}, water vapor, and wind fields at different pressure levels as well as in the ST field. In general, the PDV spatial patterns in different parameter fields share some similarities with the patterns associated with ENSO; however, important differences exist. The PDV associated upper troposphere wave train is shifted westward about 20° and is less extended zonally. This produces a different teleconnection pattern over North America and thus significant differences in ST impact. The lack of a strong PDV SST signal in the equatorial West Pacific and the relatively strong signal in the subtropical regions cause a different atmospheric overturning circulation response over the Pacific.

The spatial distribution of atmospheric heating centers offers an important clue about the dynamics of PDV. In ENSO, heating is centered in the equatorial west (central-east) Pacific during La Niña (El Niño); extratropical variations are passively caused by tropical variations through atmospheric teleconnections, consistent with the fact that the ENSO dynamical source is in the equatorial Pacific. PDV heating centers are in the subtropical west Pacific in both hemispheres (west-middle equatorial Pacific and subtropical east Pacific) in La Niña-like (El Niño-like) conditions, implying that the Pacific subtropics in both hemispheres are key regions.

Through regional analyses of the PDV, we find that the North Pacific prefers to oscillate on bidecadal or longer time scales, while the tropical and South Pacific prefer to oscillate on the decadal time scale. The North Pacific tends to lag behind the tropical and South Pacific by a few months. The similarity between the tropical and South Pacific as well as the distinct character of the North Pacific suggest that PDV may have more than one dynamical source. The variations in different regions interact through atmospheric and/or oceanic teleconnections, thus composing the Pacific pan-decadal variability.

The PDV described in this paper and the global warming (GW) trend described in Part I represent the two primary modes of global variability on time scales longer than ENSO. Our ability to cleanly separate these phenomena, one a manifestation of internal natural variability in the climate system and the other apparently a response to external climate forcing, in an EOF analysis depends crucially on the existence of multi-decadal and century-scale climate datasets. Few climate records of such length exist, but more recently acquired climate monitoring datasets now cover time periods of several decades. It is impossible to fully disentangle the contributions of natural decadal variability and externally forced climate change to the apparent "trends" seen in such datasets. However, the GW and PDV EOF and PC patterns permit us to make tentative interpretations of several such trends.

Hansen et al. (2005) compare observed ocean heat content variations from 1993-2003 to the planetary radiative energy imbalance simulated by a global climate model driven by all known external climate forcings and conclude that the upward trend in global ocean heat content is a signature of anthropogenic influences. Our PDV mode in both ST datasets has an extremely small global mean amplitude (~0.02 K) because of cancellation

between regional positive and negative anomalies, and in fact is of opposite sign in GISTEMP and ERSST.V2, indicating that its global mean impact is negligible. For comparison, a typical ENSO event has a global mean temperature impact around ±0.1K (Part I). Thus, external forcing rather than PDV seems to be the most likely explanation for the observed decadal increase in global mean ocean heat storage. However, the spatial pattern of ocean heat content change reported by Hansen et al. (2005) shows some regions of ocean heat loss over this time, most notably in the tropical east Pacific and to some extent in the eastern midlatitude Pacific basins of both hemispheres. Increased ocean heat storage occurs in the west Pacific instead. This pattern is quite similar to that of our PDV mode (Figure 1), while the GW trend mode exhibits only weak warming in most of the Pacific basin (Figure 2 of Part I). Thus, we suggest that the observed decadal ocean heat storage record is likely to reflect both the effects of external forcing, which dominate the global mean, and natural variability, which determine some elements of the regional pattern.

Chen et al. (2002) explain observed changes in the planetary radiation balance over 1985-2000 as the result of possible recent strengthening of the Hadley and Walker circulations, which causes subtropical and eastern equatorial Pacific drying and cloud clearing. As shown in Figures 5 and 6 of Part I (see also Mitas and Clement 2005, 2006), the trend in tropical overturning circulations in recent decades disagrees in different reanalyses, so a definitive statement cannot be made. The GW pattern of surface temperature trends (Figure 2 of Part I) exhibits only weak warming in most of the tropical Pacific basin relative to surrounding regions, with even a slight equatorial cooling present in the GISTEMP dataset, which might argue against a strengthening Hadley cell. On the

other hand, the PDV surface temperature pattern (Figure 2), characterized by a large area of east equatorial and subtropical Pacific cooling and moderate west Pacific warming between 30ºN-30ºS starting in the early 1990s, is of a sense that would reinforce the existing mean sea surface temperature pattern and thus might strengthen the existing tropical overturning circulations. Our results therefore appear to be consistent with the conclusion of Chen et al. (2002) that the observed top-of-atmosphere tropical radiative flux trend over this time is probably due to natural variability rather than external forcing.

Issues such as these stress the need to continue the long-term satellite monitoring of multiple climate-sensitive parameters, and to minimize artificial trends and discontinuities when assimilating these observations, until a sufficiently long reliable record is acquired to cleanly separate natural from externally forced variability. At the same time, oceanic or combined ocean-atmospheric reanalyses are needed to complete the picture of long-term climate variabilities beneath the ocean surface. As more and more of these records begin to extend across many decades, the techniques presented here and in Part I will serve as a useful template for synthesizing the information contained in these records.

Acknowledgements. This research was supported by the NASA Climate Modeling and Analysis Program. We thank Arnold Gordon, Mike Wallace, Mingfang Ting, Amy Clement and two anonymous reviewers for insightful suggestions. GISTEMP data were provided by Reto Ruedy at GISS, and can be downloaded at http://www.giss.nasa.gov/data/update/gistemp/. NOAA Extended Reconstructed SST data version 2 (ERSST.V2) were provided by the NOAA-CIRES Climate Diagnostics Center, Boulder, Colorado, USA, from their Web site at http://www.cdc.noaa.gov/. NCEP/NCAR reanalysis data were downloaded from http://www.cdc.noaa.gov/cdc/reanalysis/. The ERA-40 reanalysis monthly mean pressure level analysis data were downloaded from the European Centre for Medium-Range Weather Forecasts (ECMWF) website, http://www.ecmwf.int/products/data/archive/descriptions/e4/index.html

References:

Allan, R.P., A. Slingo and M.A. Ringer, 2002: Influence of dynamics on the changes in tropical cloud radiative forcing during the 1998 El Nino. *J. Clim.* **15**: 1979-1986.

Barnett, T.P., D.W. Pierce, M. Latif, D. Dommenget and R. Saravanan, 1999: Interdecadal interactions between the tropics and midlatitudes in the Pacific basin. *Geophys. Res. Lett.* **26**: 615-618.

Chavez, F.P., J. Ryan, S.E. Lluch-Cota and M.Ñ. C, 2003: From anchovies to sardines and back: Multidecadal change in the Pacific Ocean. *Science* **299**: 217-221.

Chen, J., B.E. Carlson and A.D. Del Genio, 2002: Evidence for strengthening of the tropical general circulation in the 1990s. *Science* **295**: 838-841.

Chen J., A.D. Del Genio, B.E. Carlson, M.G. Bosilovich, 2007: The spatiotemporal structure of 20th century climate variations in observations and reanalyses. Part I: long-term trend. *J. Clim.*, submitted

Enfield, D.B. and A.M. Mestas-Nunez, 1999: Multiscale variabilities in global sea surface temperatures and their relationships with tropospheric climate patterns. *J. Clim.* **12**: 2719-2733.

Frankignoul, C., and K. Hasselmann, 1977: Stochastic climate models. Part II. Application to SST anomalies and thermocline variability. *Tellus* **29**: 289-305.

Fyfe, J.C., and O.A. Saenko, 2007: Anthropogenic speed-up of oceanic planetary waves. *Geophys. Res. Lett.* **34**, L10706, doi:10.1029/2007GL029859.

Garreaud, R.D. and D.S. Battisti, 1999: Interannual (ENSO) and interdecadal (ENSO-like) variability in the Southern Hemisphere tropospheric circulation. *J. Clim.* **12**: 2113-2123.

Giese, B.S., S.C. Urizar and N.S. Fuckar, 2002: Southern Hemisphere Origins of the 1976 Climate Shift. *Geophys. Res. Lett.* **29**: NO. 2, 1014, doi:10.1029/2001GL013268

Graham, N., 1994: Decadal-scale climate variability in the tropical and north Pacific during the 1970s and 1980s: observations and model results. *Climate Dynamics* **10**: 135-162.

Gu, D.F. and S. Philander, 1997: Interdecadal climate fluctuations that depend on exchanges between the tropics and extratropics. *Science* **275**: 805-807.

Hansen, J., R. Ruedy, J. Glascoe and M. Sato., 1999: GISS analysis of surface temperature change. *J. Geophys. Res.-Atmos.*, **104**: 30997-31022.

Hansen, J., L. Nazarenko, R. Ruedy, Mki. Sato, J. Willis, A. Del Genio, D. Koch, A. Lacis, K. Lo, S. Menon, T. Novakov, Ju. Perlwitz, G. Russell, G.A. Schmidt, and N. Tausnev, 2005: Earth's energy imbalance: Confirmation and implications. *Science* **308**: 1431-1435, doi:10.1126/science.1110252.

Kalnay, E., M. Kanamitsu, R. Kistler, W. Collins, D. Deaven, L. Gandin, M. Iredell, S. Saha, G. White, J. Woollen, Y. Zhu, M. Chelliah, W. Ebisuzaki, W. Higgins, J. Janowiak, K.C. Mo, C. Ropelewski, J. Wang, A. Leetmaa and R. Reynolds.,1996: The NCEP/NCAR 40-year reanalysis project. *Bull. Amer. Meteorol. Soc.*, **77**: 437-471.

Kistler, R., E. Kalnay, W. Collins, S. Saha, G. White, J. Woollen, M. Chelliah, W. Ebisuzaki, M. Kanamitsu, V. Kousky, H. van den Dool, R. Jenne and M. Fiorino, 2001: The NCEP-NCAR 50-year reanalysis: Monthly means CD-ROM and documentation. *Bull. Amer. Meteorol. Soc.*, **82**: 247-267.

Knutson, T.R. and S. Manabe, 1998: Model assessment of decadal variability and trends in the tropical Pacific Ocean. *J. Clim.* **11**: 2273-2296.

Latif, M., 1998: Dynamics of interdecadal variability in coupled ocean-atmosphere models. *J. Clim.* **11**: 602-624.

Latif, M. and T.P. Barnett, 1996: Decadal Climate Variability over the North Pacific and North America: Dynamics and Predictability. *J. Clim.* **9**: 2407-2423.

Liu, Z.Y. and H.J. Yang, 2003: Extratropical control of tropical climate, the atmospheric bridge and oceanic tunnel. *Geophys. Res. Lett.* **30**: No. 5, 1230, doi:10.1029/2002GL016492

Liu, Z., L. Wu, R. Gallimore and R. Jacob, 2002: Search for the origins of Pacific decadal climate variability. *Geophys. Res. Lett.* **29**: No. 10, 1404, doi:10.1029/2001GL013735

Mantua, N.J., S.R. Hare, Y. Zhang, J.M. Wallace and R.C. Francis, 1997: A Pacific interdecadal climate oscillation with impacts on salmon production. *Bull. Amer. Meteorol. Soc.* **78**: 1069-1079.

Mantua, N.J. and S.R. Hare, 2002: The Pacific decadal oscillation. *J. Oceanogr.* **58**: 35-44.

McPhaden, M.J. and D.X. Zhang, 2002: Slowdown of the meridional overturning circulation in the upper Pacific Ocean. *Nature* **415**: 603-608.

McPhaden, M.J. and D.X. Zhang, 2004: Pacific Ocean circulation rebounds, *Geophys. Res. Lett.*, **31**, L18301, doi:10.1029/2004GL020727

Miller, A.J. and N. Schneider, 2000: Interdecadal climate regime dynamics in the North Pacific Ocean: theories, observations and ecosystem impacts. *Prog. Oceanogr.* **47**:

355-379.

Minobe, S., 1999: Resonance in bidecadal and pentadecadal climate oscillations over the North Pacific: Role in climatic regime shifts. *Geophys. Res. Lett.* **26**: 855-858.

Minobe, S., 2000: Spatio-temporal structure of the pentadecadal variability over the North Pacific. *Prog. Oceanogr.* **47**: 381-408.

Mitas, C.M., and A. Clement, 2005: Has the Hadley cell been strengthening in recent decades? *Geophys. Res. Lett.*, **32**, L03809, doi:10.1029/2004GL021765.

Mitas, C. M., and A. Clement, 2006: Recent behavior of the Hadley cell and tropical thermodynamics in climate models and reanalyses. *Geophys. Res. Lett.*, **33**, L01810, doi:10.1029/2005GL024406.

Mo, K.C., 2000: Relationships between low-frequency variability in the Southern Hemisphere and sea surface temperature anomalies. *J. Clim.* **13**: 3599-3610.

Mo, K.C. and J.N. Paegle, 2001: The Pacific-South American modes and their downstream effects. *Int. J. Climatol.*, **21**: 1211-1229.

Nitta, T. and S. Yamada, 1989: Recent warming of tropical sea-surface temperature and its relationship to the northern hemisphere circulation. *J. Meteorol. Soc. Jpn.* **67**: 375-383.

Seager, R., A. R. Karspeck, M. A. Cane, Y. Kushnir, A. Giannini, A. Kaplan, B. Kerman, and J. Velez, 2004: Predicting Pacific decadal variability, in *Earth Climate: The ocean-atmosphere interaction*, edited by C. Wang, S.-P. Xie and J. A. Carton, American Geophysical Union, Washington DC, 105-120.

Smith, T.M. and R.W. Reynolds, 2003: Extended reconstruction of global sea surface temperatures based on COADS data (1854-1997). *J. Clim.* **16**: 1495-1510.

Smith, T.M. and R.W. Reynolds, 2004: Improved Extended Reconstruction of SST (1854-1997). *J. Clim.* **17**: 2466-2477.

Timmermann, A., S.I. An, U. Krebs and H. Goosse, 2005: ENSO suppression due to weakening of the North Atlantic thermohaline circulation. *J. Clim.* **18**: 3122-3139.

Tourre, Y.M., B. Rajagopalan, Y. Kushnir, M. Barlow and W.B. White, 2001: Patterns of coherent decadal and interdecadal climate signals in the Pacific Basin during the 20th century. *Geophys. Res. Lett.* **28**: 2069-2072.

Trenberth, K.E., 1990: Recent observed interdecadal climate changes in the northern hemisphere. *Bull. Amer. Meteorol. Soc.* **71**: 988-993.

Trenberth, K.E. and J.W. Hurrell, 1994: Decadal atmosphere-ocean variations in the Pacific. *Clim. Dyn.* **9**: 303-319.

Trenberth, K.E., G.W. Branstator, D. Karoly, A. Kumar, N.C. Lau and C. Ropelewski, 1998: Progress during TOGA in understanding and modeling global teleconnections associated with tropical sea surface temperatures. *J. Geophys. Res.-Oceans* **103**: 14291-14324.

Uppala, S.M., P.W. Kållberg, A.J. Simmons, U. Andrae V. da Costa Bechtold, M. Fiorino, J.K. Gibson, J. Haseler, A. Hernandez, G.A. Kelly, X. Li, K. Onogi, S. Saarinen, N. Sokka, R.P. Allan, E. Andersson, K. Arpe, M.A. Balmaseda, A.C.M. Beljaars, L. van de Berg, J. Bidlot, N. Bormann, S. Caires, F. Chevallier, A. Dethof, M. Dragosavac, M. Fisher, M. Fuentes, S. Hagemann, E. Hólm, B.J. Hoskins, L. Isaksen, P.A.E.M. Janssen, R. Jenne, A.P. McNally, J.-F. Mahfouf, J.-J. Morcrette, N.A. Rayner, R.W. Saunders, P. Simon, A. Sterl, K.E. Trenberth, A. Untch, D.

Vasiljevic, P. Viterbo, and J. Woollen, 2005: The ERA-40 re-analysis. *Quart. J. R. Meteorol. Soc.*, 131: 2961-3012. doi:10.1256/qj.04.176

Wang, C.Z., 2002: Atmospheric circulation cells associated with the El Nino-Southern Oscillation. *J. Clim.* **15**: 399-419.

White, W.B., Y.M. Tourre, M. Barlow and M. Dettinger, 2003: A delayed action oscillator shared by biennial, interannual, and decadal signals in the Pacific Basin. *J. Geophys. Res.-Oceans* **108**: NO. C3, 3070, doi:10.1029/2002JC001490,

Wu, L.X., F. He and Z.Y. Liu, 2005: Coupled ocean-atmosphere response to north tropical Atlantic SST: tropical Atlantic dipole and ENSO. *Geophys. Res. Lett.* **32**: L21712, doi:10.1029/2005GL024222.

Wu, L., Z. Liu, R. Gallimore, R. Jacob, D. Lee and Y. Zhong, 2003: Pacific decadal variability: The tropical Pacific mode and the North Pacific mode. *J. Clim.* **16**: 1101-1120.

Zhang, Y., J.M. Wallace and D.S. Battisti, 1997: ENSO-like interdecadal variability: 1900-93. *J. Clim.* **10**: 1004-1020.

Figure Captions

Figure 1. The Pacific Pan-Decadal mode for the 1900–2003 ENSO-removed EOF analyses based on GISTEMP and ERSST.V2. This mode explains 7.0% and 10.5% of the total variance in the ENSO-removed annually smoothed anomaly data of GISTEMP and ERSST.V2, respectively. Top: the principal components (PC) from GISTEMP (black solid) and ERSST.V2 (red dashed). The correlation coefficient between the two PCs is 0.95. The PCs are scaled to represent the mean ST change associated with this mode. Middle: the EOF spatial pattern from GISTEMP. Bottom: the EOF spatial pattern from ERSST.V2. Each grid of the EOF spatial patterns is scaled to represent the range of the local temperature change associated with the PC time series. We draw the plots so that the PC values are negative after 1976 (thus, the La Niña-like status is shown by a positive value). Accordingly, the EOF spatial patterns are shown with negative values in the tropical Pacific regions and positive values in the middle latitudes of both North and South Pacific regions.

Figure 2. Comparison of PDV and ENSO spatial patterns from GISTEMP. Upper: the PDV spatial pattern from 1900–2003 ENSO-removed EOF analysis. Middle: the ENSO spatial pattern, being the range of ENSO signal at each grid box based on the algorithm introduced in Part I. Bottom left: the difference between the absolute value of the standardized ENSO and the PDV signal from GISTEMP (|ENSOsG|-|PDVsG|). Bottom right: the ratio of |ENSOsG|-|PDVsG| to |PDVsG-PDVsE|, that is, the absolute value of the difference between the standardized PDV signals from GISTEMP and ERSST.V2.

Figure 3. Upper. Red solid line: The PC time series of the PDV (second mode, 9.6% variance explained) mode of the 1970–2003 ENSO-removed combined EOF analysis

(NCEP1-40p) based on NCEP/NCAR. Black dashed line: the PC time series of the PDV (second mode, 9.1% variance explained) mode of the 1970–2002 ENSO-removed combined EOF analysis (ERA40-40p) based on ERA-40. For reference, the 1970–2003 segments of the PDV mode PCs of the 1900–2003 ENSO-removed EOF analyses based on ERSST.V2 (green triangle up) and GISTEMP (orange square) are also shown. The correlation coefficient between the NCEP1-40p PDV PC and the GISTEMP (ERSST.V2) PDV PC is 0.76 (0.88). Lower: The negative Niño-3.4 index (black) and N34h index (red dashed).

Figure 4. The representative spatial patterns of the dynamic field variations associated with ENSO (left) and PDV (right). Top: the 300hPa horizontal wind field; middle: the 500hPa vertical velocity field; a positive value indicates descending motion; bottom: the 850hPa horizontal wind field.

Figure 5. T_{air} variation at pressure levels from 1000hPa to 300hPa associated with ENSO (left) and PDV (right).

Figure 6. Q variation at pressure levels from 1000hPa to 400hPa associated with ENSO (left) and PDV (right).

Figure 7. Lower three plots: the PDV spatial patterns from regional EOF analyses based on the ERSST.V2 after both ENSO and GW trend are removed. The three regions are South Pacific (60°S-20°S, S62), tropical Pacific (20°S-20°N, M22), and North Pacific (20°N-60°N, N26). Top plot: the original PDV spatial pattern based on the ENSO-removed 60°S-60°N (M60) EOF analysis.

Figure 8. Top: the PDV PCs from different EOF analyses based on ERSST.V2 corresponding with the spatial patterns shown in Figure 7. Middle: the spectra of the PCs

shown in the top plot. Bottom: the cross-correlations between the PCs; a positive value indicates that the first time series lags behind the second time series. For example, M60 lags M22 by one month, and S62 leads N26 by 5 months.

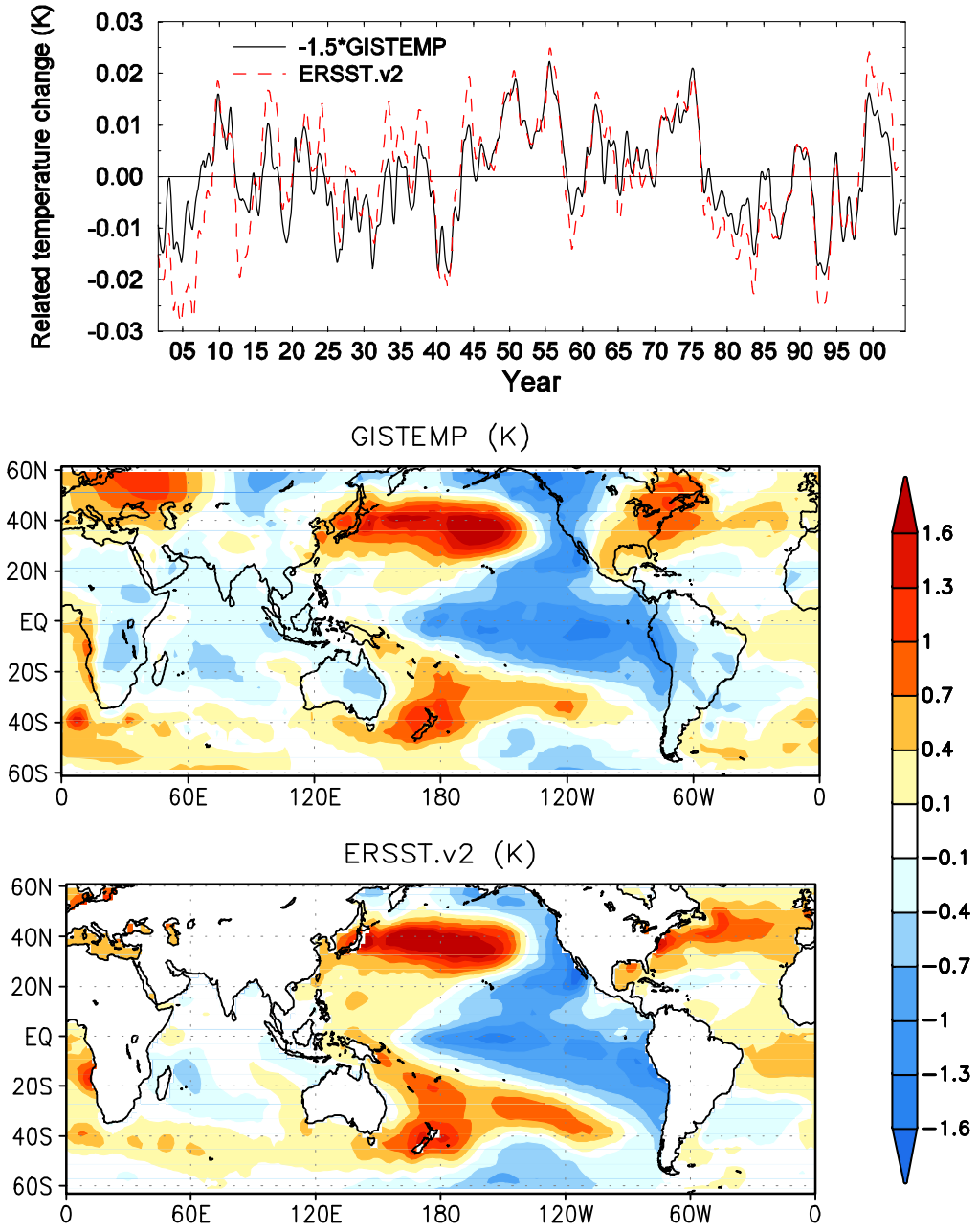

Figure 1. The Pacific Pan-Decadal mode for the 1900–2003 ENSO-removed EOF analyses based on GISTEMP and ERSST.V2. This mode explains 7.0% and 10.5% of the total variance in the ENSO-removed annually smoothed anomaly data of GISTEMP and ERSST.V2, respectively. Top: the principal components (PC) from GISTEMP (black solid) and ERSST.V2 (red dashed). The correlation coefficient between the two PCs is 0.95. The PCs are scaled to represent the mean ST change associated with this mode. Middle: the EOF spatial pattern from GISTEMP. Bottom: the EOF spatial pattern from ERSST.V2. Each grid of the EOF spatial patterns is scaled to represent the range of the local temperature change associated with the PC time series. We draw the plots so that the PC values are negative after 1976 (thus, the La Niña-like status is shown by a positive value). Accordingly, the EOF spatial patterns are shown with negative values in the tropical Pacific regions and positive values in the middle latitudes of both North and South Pacific regions.

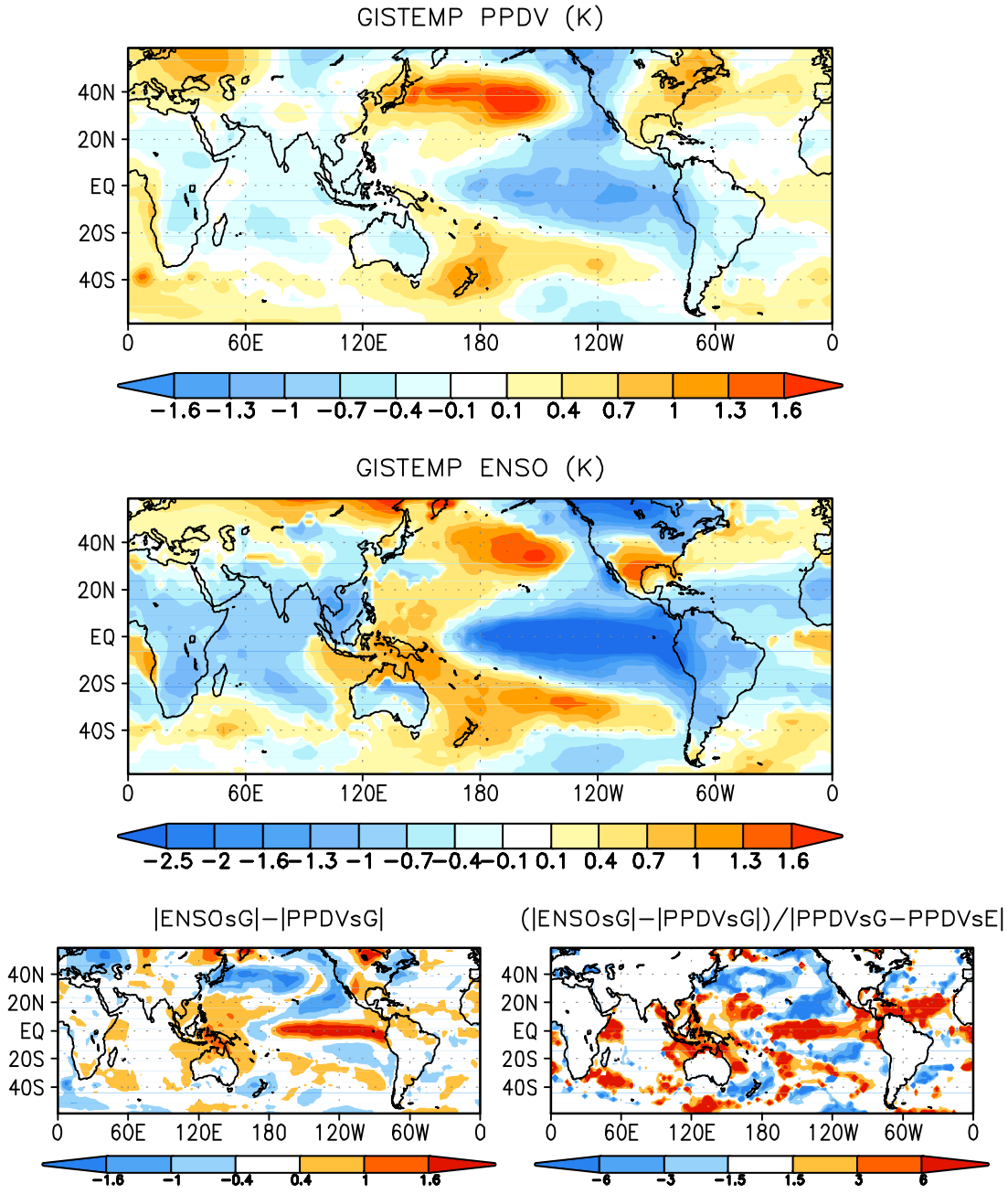

Figure 2. Comparison of PDV and ENSO spatial patterns from GISTEMP. Upper: the PDV spatial pattern from 1900–2003 ENSO-removed EOF analysis. Middle: the ENSO spatial pattern, being the range of ENSO signal at each grid box based on the algorithm introduced in Part I. Bottom left: the difference between the absolute value of the standardized ENSO and the PDV signal from GISTEMP (|ENSOsG|-|PDVsG|). Bottom right: the ratio of |ENSOsG|-|PDVsG| to |PDVsG-PDVsE|, that is, the absolute value of the difference between the standardized PDV signals from GISTEMP and ERSST.V2.

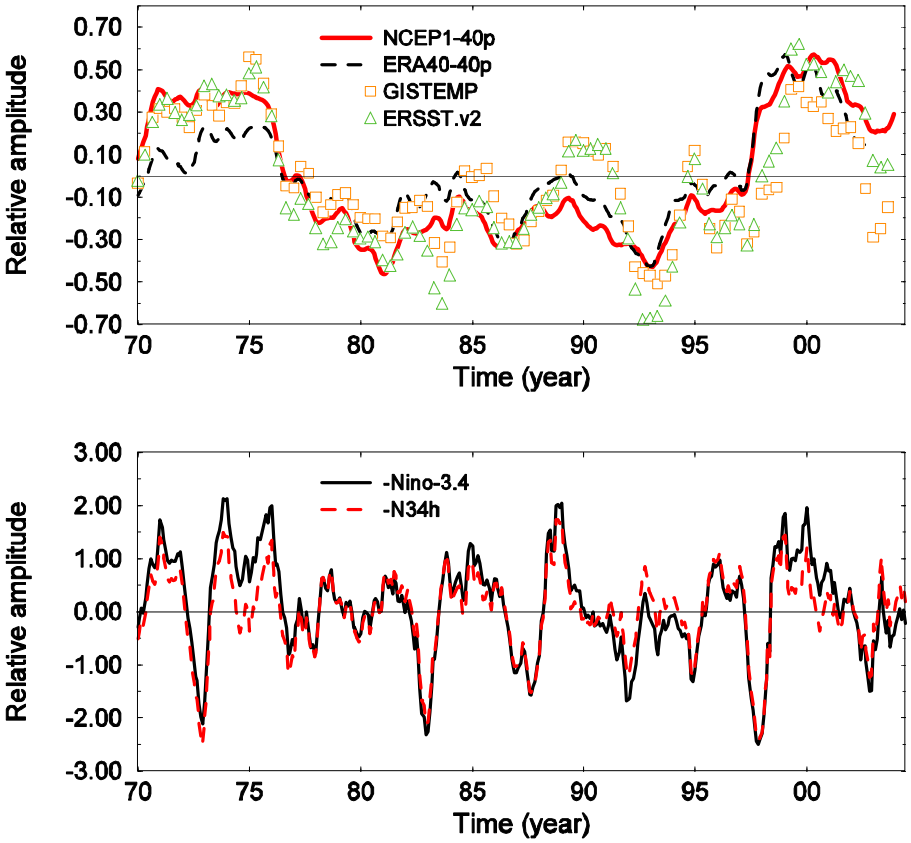

Figure 3. Upper. Red solid line: The PC time series of the PDV (second mode, 9.6% variance explained) mode of the 1970–2003 ENSO-removed combined EOF analysis (NCEP1-40p) based on NCEP/NCAR. Black dashed line: the PC time series of the PDV (second mode, 9.1% variance explained) mode of the 1970–2002 ENSO-removed combined EOF analysis (ERA40-40p) based on ERA-40. For reference, the 1970–2003 segments of the PDV mode PCs of the 1900–2003 ENSO-removed EOF analyses based on ERSST.V2 (green triangle up) and GISTEMP (orange square) are also shown. The correlation coefficient between the NCEP1-40p PDV PC and the GISTEMP (ERSST.V2) PDV PC is 0.76 (0.88). Lower: The negative Niño-3.4 index (black) and N34h index (red dashed).

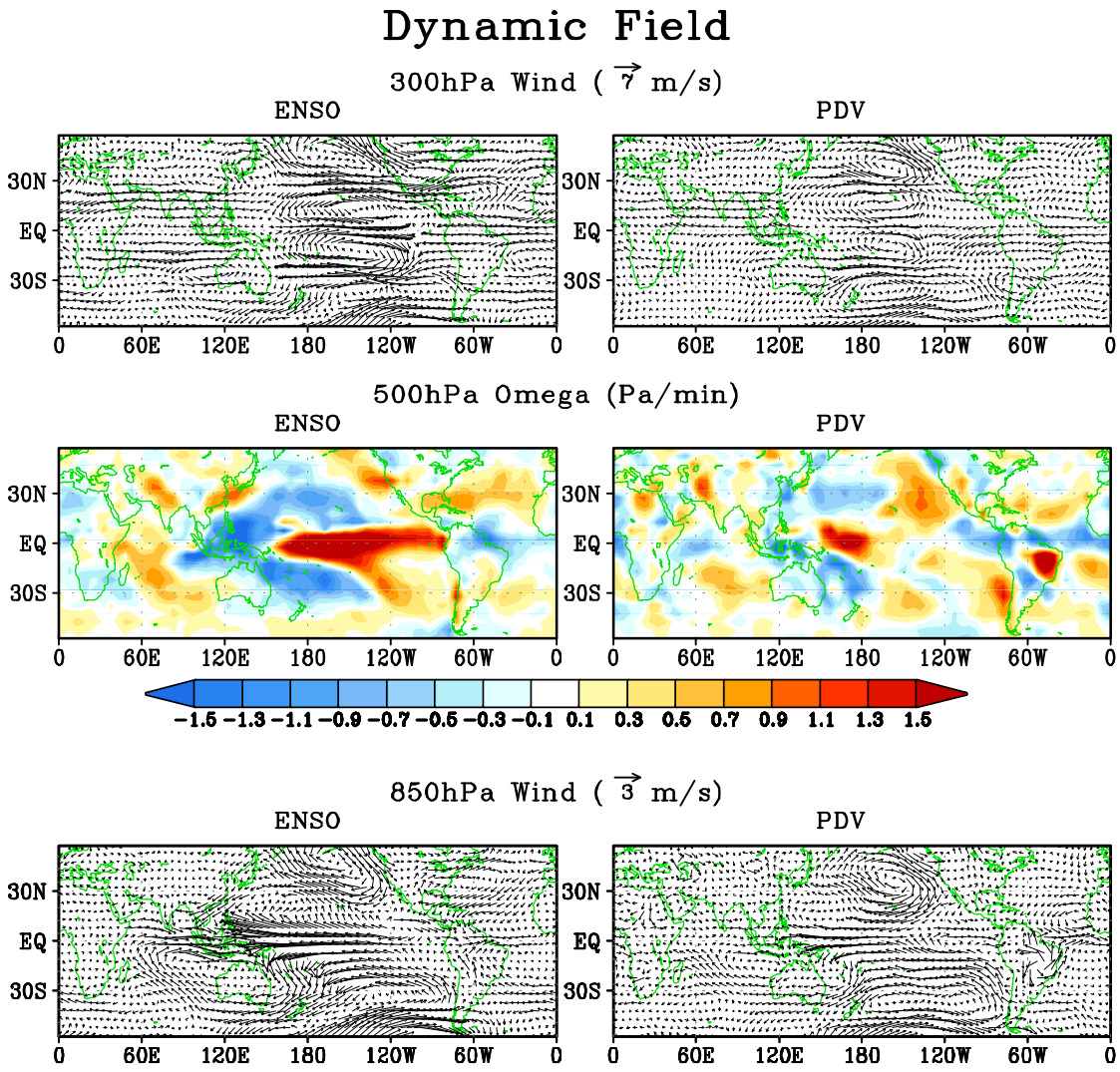

Figure 4. The representative spatial patterns of the dynamic field variations associated with ENSO (left) and PDV (right). Top: the 300hPa horizontal wind field; middle: the 500hPa vertical velocity field; a positive value indicates descending motion; bottom: the 850hPa horizontal wind field.

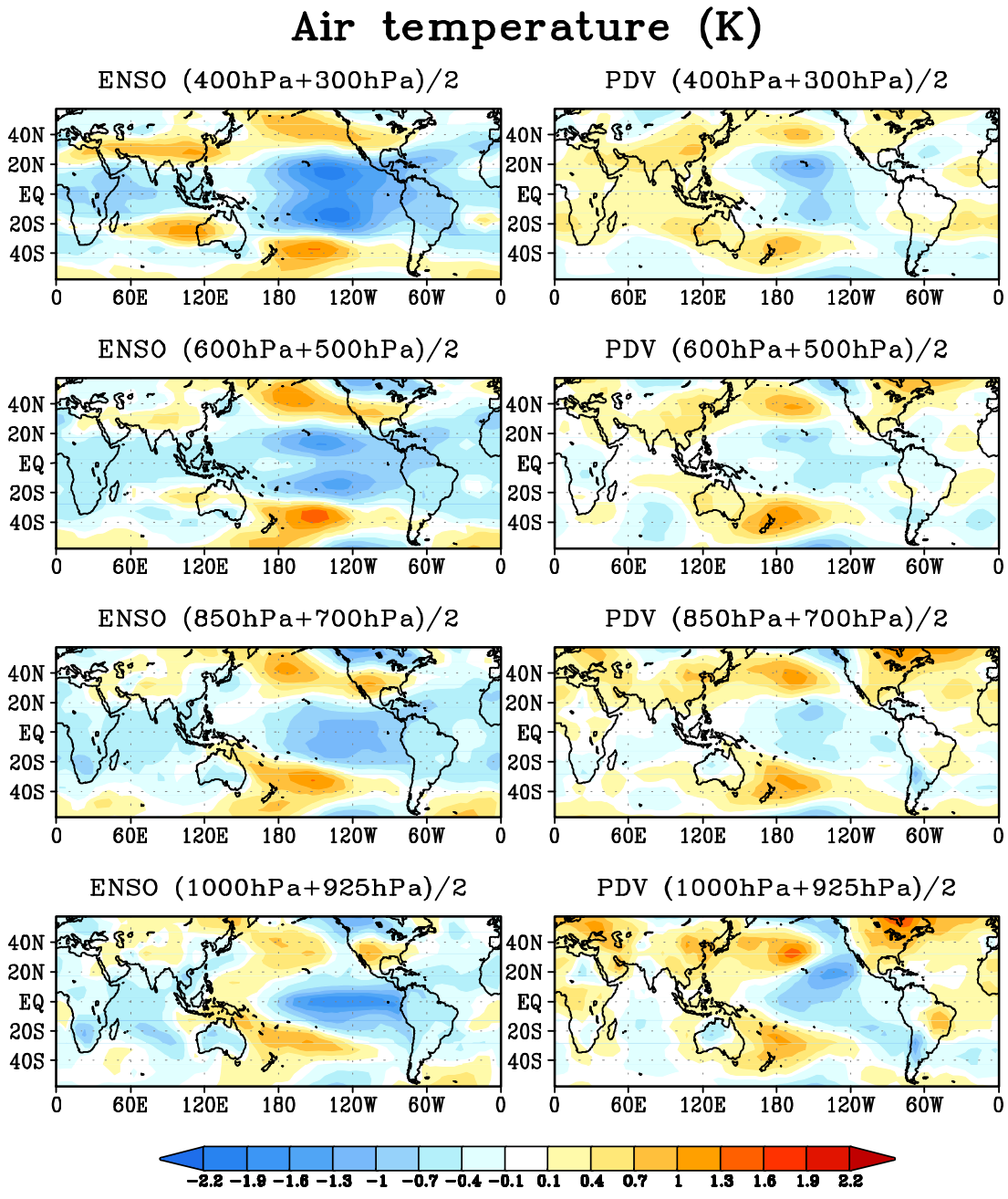

Figure 5. T_{air} variation at pressure levels from 1000hPa to 300hPa associated with ENSO (left) and PDV (right).

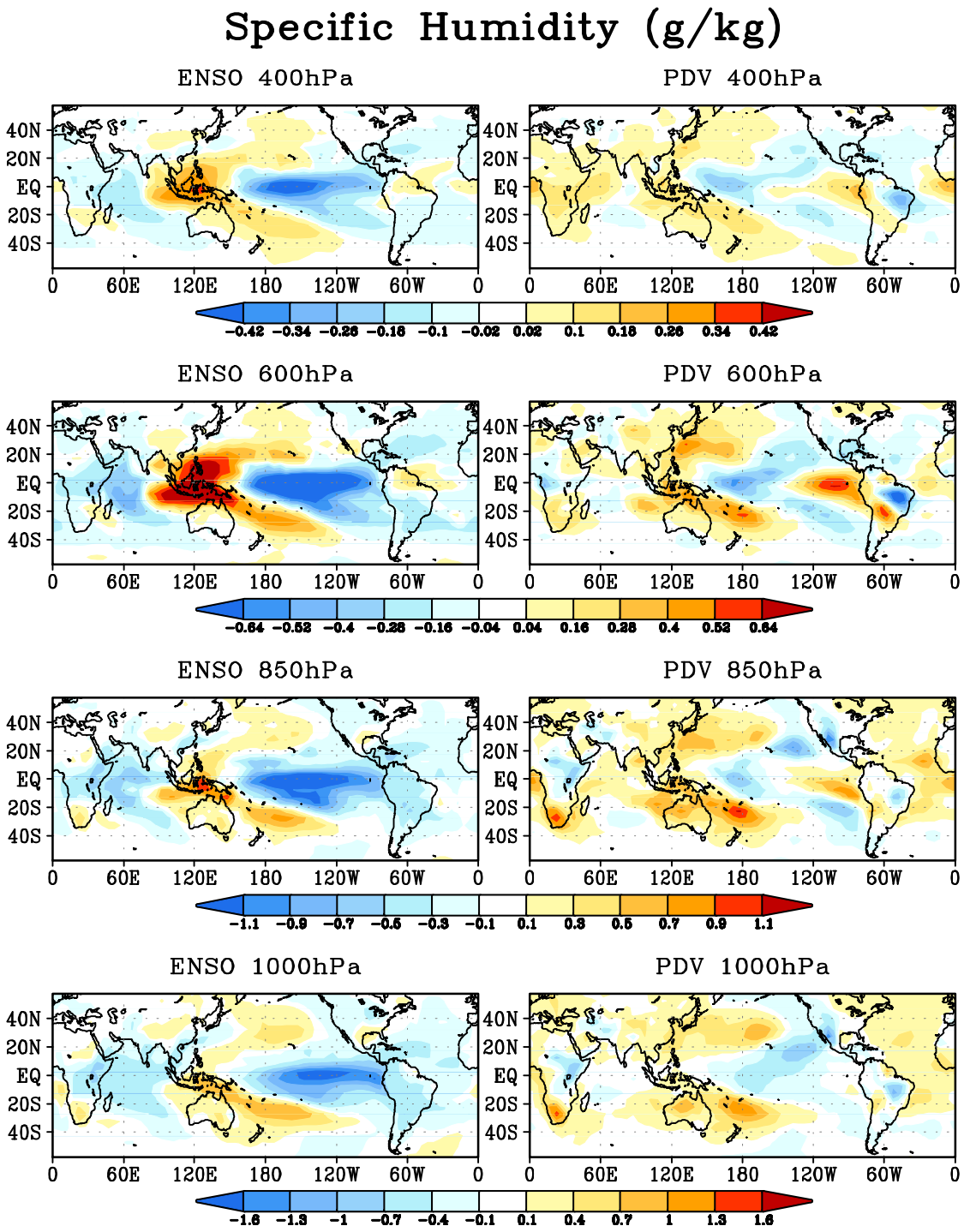

Figure 6. Q variation at pressure levels from 1000hPa to 400hPa associated with ENSO (left) and PDV (right).

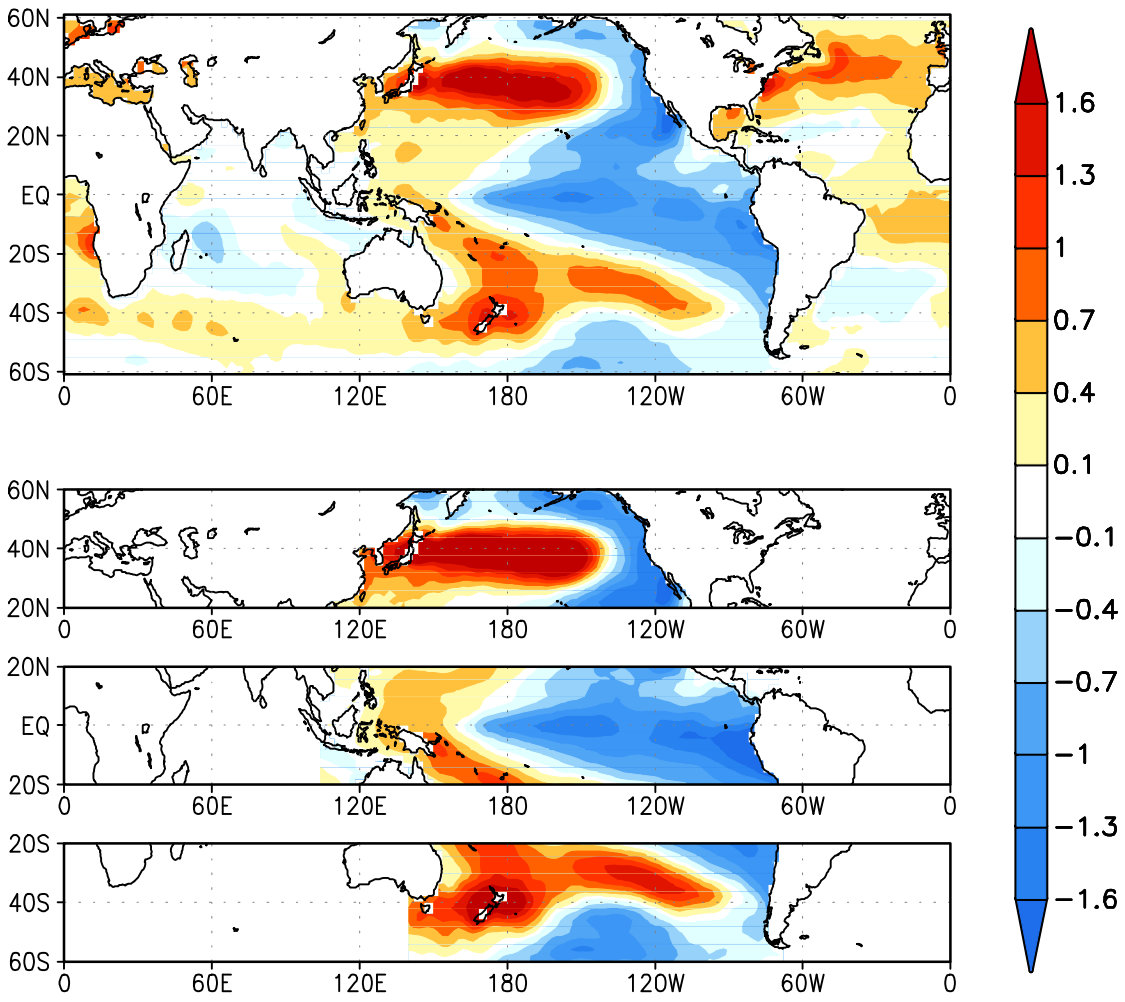

Figure 7. Lower three plots: the PDV spatial patterns from regional EOF analyses based on the ERSST.V2 after both ENSO and GW trend are removed. The three regions are South Pacific (60°S-20°S, S62), tropical Pacific (20°S-20°N, M22), and North Pacific (20°N-60°N, N26). Top plot: the original PDV spatial pattern based on the ENSO-removed 60°S-60°N (M60) EOF analysis.

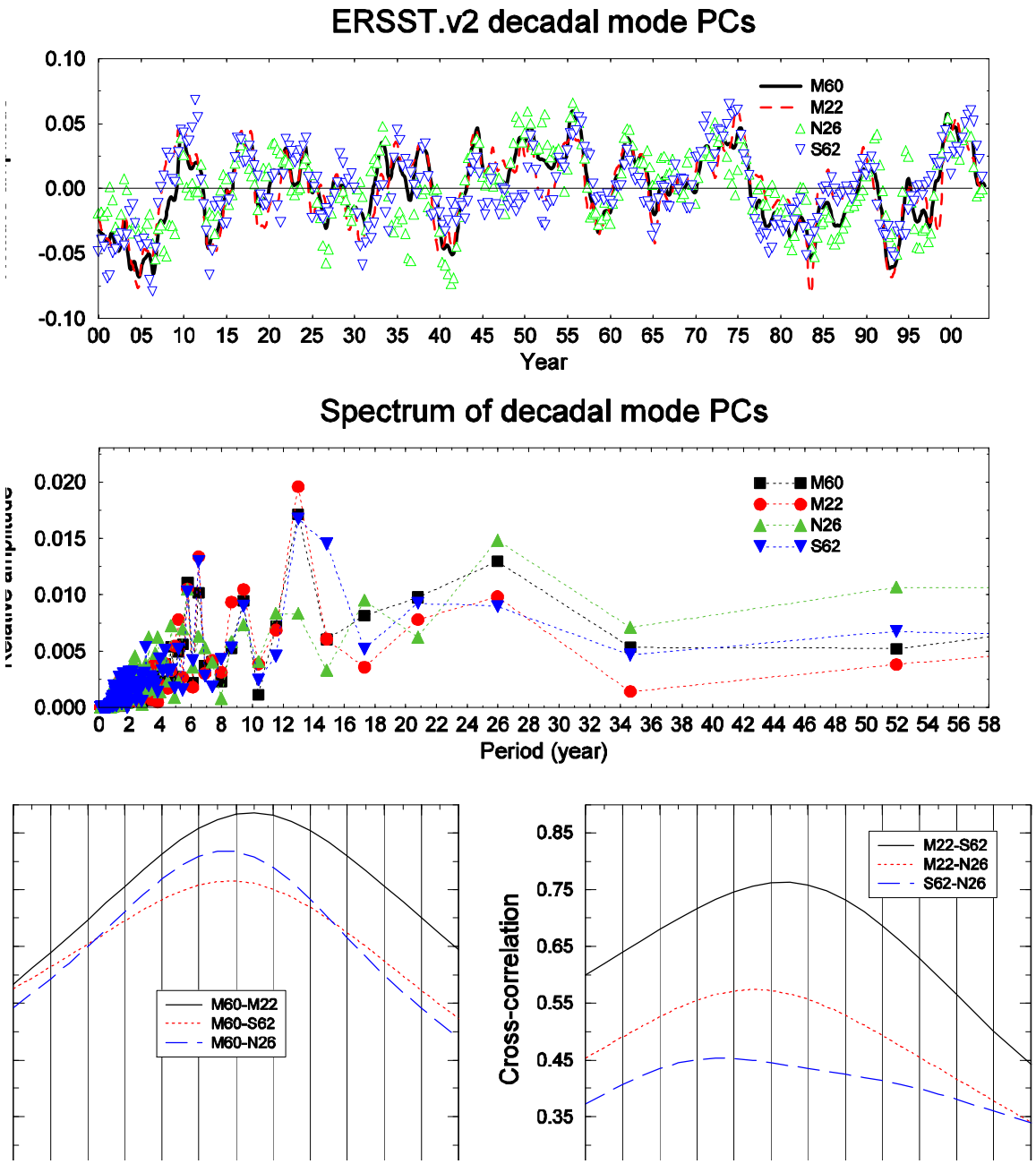

Figure 8. Top: the PDV PCs from different EOF analyses based on ERSST.V2 corresponding with the spatial patterns shown in Figure 7. Middle: the spectra of the PCs shown in the top plot. Bottom: the cross-correlations between the PCs; a positive value indicates that the first time series lags behind the second time series. For example, M60 lags M22 by one month, and S62 leads N26 by 5 months.

Table 1. The correlation coefficients between PDV and ENSO in atmospheric spatial patterns based on NCEP/NCAR reanalysis data.

	1000hPa	925hPa	850hPa	700hPa	600hPa	500hPa	400hPa	300hPa
T	0.52	0.50	0.47	0.39	0.42	0.50	0.42	0.19
U	0.62	0.61	0.64	0.59	0.60	0.58	0.60	0.69
V	0.39	0.36	0.35	0.36	0.36	0.34	0.37	0.42
ω	0.38	0.31	0.26	0.20	0.20	0.18	0.20	0.26
q	0.57	0.28	0.41	0.47	0.18	0.33	0.36	0.42

Table 2. The correlation coefficients between PDV and ENSO in atmospheric spatial patterns based on ERA-40 reanalysis data.

	1000hPa	925hPa	850hPa	700hPa	600hPa	500hPa	400hPa	300hPa
T	0.27	0.24	0.28	0.38	0.34	0.44	0.58	0.61
U	0.54	0.55	0.57	0.52	0.49	0.49	0.53	0.55
V	0.23	0.25	0.26	0.21	0.16	0.13	0.18	0.25
ω	0.16	0.17	0.20	0.25	0.29	0.29	0.29	0.31
q	0.30	0.38	0.20	0.26	0.39	0.39	0.26	0.03

Table 3. The correlation coefficients between NCEP/NCAR reanalysis and ERA-40 reanalysis in ENSO spatial patterns.

	1000hPa	925hPa	850hPa	700hPa	600hPa	500hPa	400hPa	300hPa
T	0.87	0.84	0.86	0.87	0.83	0.83	0.91	0.93
U	0.89	0.90	0.92	0.90	0.87	0.87	0.89	0.91
V	0.77	0.79	0.81	0.79	0.76	0.75	0.76	0.79
ω	0.38	0.65	0.72	0.78	0.79	0.80	0.82	0.85
q	0.88	0.83	0.74	0.82	0.86	0.87	0.87	0.83

Table 4. The correlation coefficients between NCEP/NCAR reanalysis and ERA-40 reanalysis in PDV spatial patterns.

	1000hPa	925hPa	850hPa	700hPa	600hPa	500hPa	400hPa	300hPa
T	0.76	0.72	0.66	0.72	0.74	0.78	0.74	0.43
U	0.74	0.75	0.78	0.77	0.76	0.81	0.84	0.83
V	0.58	0.54	0.51	0.60	0.60	0.61	0.63	0.65
ω	-0.02	0.17	0.26	0.32	0.41	0.47	0.52	0.59
q	0.63	0.54	0.52	0.46	0.54	0.59	0.47	0.01